

Environmental Science Nano

Accepted Manuscript



This is an *Accepted Manuscript*, which has been through the Royal Society of Chemistry peer review process and has been accepted for publication.

Accepted Manuscripts are published online shortly after acceptance, before technical editing, formatting and proof reading. Using this free service, authors can make their results available to the community, in citable form, before we publish the edited article. We will replace this *Accepted Manuscript* with the edited and formatted *Advance Article* as soon as it is available.

You can find more information about *Accepted Manuscripts* in the [Information for Authors](#).

Please note that technical editing may introduce minor changes to the text and/or graphics, which may alter content. The journal's standard [Terms & Conditions](#) and the [Ethical guidelines](#) still apply. In no event shall the Royal Society of Chemistry be held responsible for any errors or omissions in this *Accepted Manuscript* or any consequences arising from the use of any information it contains.

1 Manuscript for *Environmental Science: Nano*

2

3 **A novel two-compartment barrier model for investigating**
4 **nanoparticle transport in fish intestinal epithelial cells**

5

6 Mark Geppert^{1#}, Laura Sigg^{1,2} and Kristin Schirmer*^{1,2,3}

7

8 ¹Eawag - Swiss Federal Institute of Aquatic Science and Technology, 8600 Dübendorf,
9 Switzerland

10 ²ETH Zürich, Swiss Federal Institute of Technology, Institute of Biogeochemistry and Pollutant
11 Dynamics, 8092 Zürich, Switzerland

12 ³EPF Lausanne, School of Architecture, Civil and Environmental Engineering, 1015 Lausanne,
13 Switzerland

14

15 [#]current address: University of Salzburg, Department of Molecular Biology, 5020 Salzburg,
16 Austria

17

18

19 *Corresponding author:

20 Kristin Schirmer

21 Environmental Toxicology

22 Eawag, Swiss Federal Institute of Aquatic Science and Technology

23 Überlandstrasse 133

24 P.O. Box 611

25 8600 Dübendorf, Switzerland

26 kristin.schirmer@eawag.ch

27

28 **Abstract**

29 We introduce a novel *in vitro* rainbow trout intestinal barrier model and demonstrate its
30 suitability for investigating nanoparticle transport across the intestinal epithelium. Rainbow
31 trout (*Oncorhynchus mykiss*) intestinal cells (RTgutGC) were grown as monolayers on
32 permeable supports leading to a two-compartment intestinal barrier model consisting of a
33 polarized epithelium, dividing the system into an upper (apical) and a lower (basolateral)
34 compartment, and thereby mimicking the intestinal lumen and the portal blood, respectively.
35 The cells express the tight junction protein ZO-1 and build up a transepithelial electrical
36 resistance comparable to the *in vivo* situation. Fluorescent polystyrene nanoparticles (PS-NPs;
37 average hydrodynamic diameter: 73 ± 18 nm) were accumulated by RTgutGC cells in a time-,
38 temperature and concentration dependent manner. Uptake of PS-NPs was confirmed using
39 fluorescence microscopy. Cells formed an efficient barrier largely preventing the translocation
40 of PS-NPs to the basolateral compartment. Taken together, these data demonstrate the
41 suitability of the *in vitro* barrier model to study the effects of nanoparticles in fish intestinal
42 epithelial cells.

43

44

45

46

47

48

49

50

51

52 **Nano impact**

53 The rapid growth of nanotechnology requires a close investigation of potential hazardous
54 effects of these new materials not only to humans but also to the ecosystem. Our study
55 introduces the first *in vitro* fish intestinal barrier model based on a rainbow trout intestinal cell
56 line and demonstrates its suitability for studying the role of fish intestinal epithelial cells as a
57 barrier for nanoparticle uptake and transport. We show that nanoparticles can be accumulated in
58 rainbow trout intestinal epithelial cells, but that their transport through the epithelium is largely
59 prevented. The developed model system has great potential in a tiered assessment approach. It
60 can be applied for screening particles with respect to their transferability through the fish
61 intestinal epithelium but as well for mechanistic investigations of particle effects on the
62 molecular and cellular level.

63

64

65

66

67

68

69

70

71

72

73

74

75 Introduction

76 The rapid increase in production, use and release of engineered nanoparticles (ENPs) demands
77 for a thorough investigation of their potential ecotoxicological effects. Considering the aquatic
78 environment, both marine and freshwaters are known to act as sinks for ENPs as they do also
79 for metals and other environmental pollutants¹⁻⁴. Fish are frequently used model organisms for
80 investigation of the effects of chemicals and ENPs to the aquatic environment. Two major
81 pathways for ENP uptake into fish exist: dietary uptake across the gastro-intestinal system or
82 waterborne uptake across the gill epithelium^{1,5}.

83

84 Cell lines derived from Rainbow trout (*Oncorhynchus mykiss*) are a frequently used model for
85 studying the effects of nanoparticles to fish⁶⁻⁸. The cell lines used in these studies came from
86 different tissues, such as the gill, gut, liver, brain or gonads. However, none of these studies has
87 explored the barrier potential of rainbow trout intestinal epithelial cells.

88

89 The gut of fish is a multifunctional organ not only involved in absorption of nutrients but also
90 in ionic and osmotic regulation⁹. Our current knowledge on this organ comes from *in vivo* and
91 *ex vivo* studies such as the gut sac preparation^{10, 11}. However, the translocation of ENPs across
92 the gut is poorly understood so far. In an *in vivo* study, Gaiser and co-workers¹ exposed carp
93 (*Cyprinus Carpio*) to silver nanoparticles and measured significant increases of silver contents
94 in liver and intestine, suggesting that silver nanoparticles or at least silver ions are being
95 translocated across the intestinal barrier. Al-Jubory and Handy¹² demonstrated the uptake of
96 titanium across the intestine from TiO₂ nanoparticle exposure by using *ex vivo* static gut sac
97 preparations and isolated perfused intestines. Although, these two exposure systems have their
98 strengths, an *in vitro* cell-line based intestinal barrier model would be a great advantage for
99 detailed investigation of ENP uptake and transepithelial transport, especially with regards to the

100 molecular and cellular mechanisms and for animal-free higher throughput screening. It
101 therefore is our aim to provide the means to investigate the uptake and translocation of ENPs in
102 such a fish intestinal barrier model.

103

104 There is a given number of studies describing nanoparticle translocation in the human-derived
105 Caco-2 cell model established by Hidalgo and colleagues¹³. Koeneman and co-workers¹⁴
106 incubated an intestinal barrier model of Caco-2 cells with TiO₂ nanoparticles and showed that
107 TiO₂ was able to penetrate into and through the cells without disrupting junctional complexes.
108 Similar findings were presented for polystyrene nanoparticles on Caco-2 cells¹⁵ or Caco-
109 2/HT29-MTX co-cultures¹⁶. In an earlier report, des Rieux and colleagues¹⁷ investigated the
110 transport of polystyrene nanoparticles in a co-culture model of Caco-2, Raji and epithelial
111 microfold cells (M cells¹⁸). They concluded that the nanoparticle transport by M cells occurs by
112 the transcellular route and is dependent on energy and endocytotic processes¹⁷. Contrasting
113 results were reported for iron oxide nanoparticles, which were not transported at detectable
114 levels across two different Caco-2 intestinal barrier models¹⁹. However, it was shown that iron
115 oxide nanoparticles can induce reorganization and distortion of microvilli and disruption of
116 junctions in Caco-2 cells which lead to a loss in epithelial integrity²⁰.

117

118 We report here the development of a novel two-compartment intestinal barrier model using the
119 rainbow trout intestinal cell line RTgutGC²¹. We show that the model is suitable for
120 investigation of nanoparticle translocation and demonstrate the function of RTgutGC cells as a
121 barrier, which largely prevents translocation of fluorescent polystyrene nanoparticles across the
122 intestinal epithelium.

123

124 **Materials and methods**

125 *Materials*

126 Leibovitz L-15 medium, Versene, CellMask®, 4',6'-diaminido-2-phenylindole (DAPI) and the
127 Alexa Fluor® 488-coupled monoclonal zonula occludence (ZO-1) antibody were purchased
128 from Invitrogen (Basel, Switzerland), fetal bovine serum (FBS) and gentamycin were from
129 PAA (Basel, Switzerland), Trypsin was from Biowest (Nuaille, France). All other chemicals
130 were from Sigma Aldrich (Buchs, Switzerland) and of high purity. 75 cm² cell culture flasks
131 were from TPP (Transadingen, Switzerland) and 24-well cell culture plates from Greiner-bio-
132 one (Frickenhausen, Germany). Permeable membrane supports with PET-membranes and pore
133 sizes of 0.4, 1 and 3 µm were from Greiner-bio-one (Frickenhausen, Germany).

134

135 *Nanoparticles*

136 Fluoresbrite® carboxylated fluorescent polystyrene nanoparticles (PS-NPs) were purchased
137 from Polysciences (Warrington, PA, United States). These particles have been shown to be
138 suitable for investigation of transepithelial NP-transport in an *in vitro* human intestinal barrier
139 model¹⁶. According to the supplier, the particles appear as 2.5% (25 g/L) aqueous dispersion
140 containing 3.64×10^{14} particles/mL with a mean particle diameter of 50 nm and a negative
141 surface charge.

142

143 *Characterization and quantification of PS-NPs*

144 The aqueous PS-NP dispersion was diluted in water or the respective medium (see supporting
145 information for media description) to a final concentration of 10 mg/L and 1 mL of this diluted
146 dispersion was injected into a Malvern DTS-1061 capillary cell (Herrenberg, Germany) and
147 analyzed for hydrodynamic size and zeta-potential with a Malvern ZetaSizer Nano ZS

148 (Herrenberg, Germany). Quantification of PS-NPs in media and cell lysates was performed by
149 fluorescence measurement ($\lambda_{\text{ex}} = 441 \text{ nm}$, $\lambda_{\text{em}} = 486 \text{ nm}$) using a multiwell plate reader (Infinite
150 2000, Tecan, Maennedorf, Switzerland). Amounts of PS-NPs were calculated from
151 fluorescence intensities obtained in media/cell lysates compared to fluorescence intensities
152 obtained in standard curves of PS-NP dilutions in the respective media (see supporting
153 information).

154

155 *Cell cultures*

156 Rainbow trout intestinal cells (RTgutGC) were isolated from the gut of a small female rainbow
157 trout as described previously²¹. It has been shown that RTgutGC cells have the properties
158 consistent with immortal cell lines and that they are able to be subcultured for at least 100
159 times²¹. For routine culture, RTgutGC cells were kept in 75 cm² flasks in complete medium (L-
160 15/FBS, see supporting information) and incubated at 19 °C at normal atmosphere. Medium
161 change was performed every week. Cells that reached confluency were trypsinized and
162 subcultured in a 1:3 ratio. For nanoparticle exposure experiments, cells were trypsinized,
163 counted and seeded at a density of 62500 cells/cm² in 300 μL L-15/FBS in the apical
164 compartment of a permeable membrane support. The basolateral compartment was filled with 1
165 mL L-15/FBS and the cells were grown for at least 3 weeks at 19 °C before particle exposure
166 experiments. Medium change of both, apical and basolateral medium was performed every
167 week. As a control, empty membranes (cell-free) were filled with 300 μL L-15/FBS (apical
168 chamber) and 1 mL L-15/FBS (basolateral chamber) and treated identically.

169

170 *Experimental incubation*

171 Cells were taken out of the incubator and the basolateral and apical media were removed. The
172 cells (apical side) were washed twice with 300 μ L exposure medium (L-15/ex, see supporting
173 information) before adding 300 μ L or L-15/ex containing the desired concentrations of PS-NPs.
174 Finally, the basolateral chamber was re-filled with 1 mL complete medium (L-15/FBS, see
175 supporting information) and cells incubated in the incubator (19 $^{\circ}$ C) or fridge (4 $^{\circ}$ C) for the
176 desired time-period. After the incubation, both media were collected and the cells washed twice
177 with 300 μ L phosphate-buffered saline (PBS). Finally, cells were lysed by incubating them in
178 300 μ L 50 mM NaOH for 2 h on a shaker (Geppert et al. 2011). Lysates, apical and basolateral
179 media were analyzed for their fluorescence. As controls, cell-free membranes were treated
180 identically.

181

182 *TEER measurement*

183 Transepithelial electrical resistance (TEER) was measured using the EVOM Voltohmmeter in
184 combination with the Endohm-6 chamber (World Precision Instruments, Berlin, Germany).
185 TEER of RTgutGC cells was calculated by subtracting the blank values (obtained on cell-free
186 membranes) from the values obtained on membranes containing cells.

187

188 *Fluorescence microscopy*

189 Tight junction staining was performed as follows: Cells were taken out of the incubator and
190 washed twice for 5 min with 300 μ L PBS and then fixed for 10 min with 300 μ L of 3.7%
191 formaldehyde at 4 $^{\circ}$ C. Cells were washed twice for 5 min with 300 μ L PBS and then incubated
192 with PBS containing 0.5% Triton X-100 and 5% goat serum for 30 min at 4 $^{\circ}$ C in the dark.
193 Cells were washed thrice with 300 μ L of 0.1% Triton X-100 in PBS for 5 min each and
194 incubated overnight at 4 $^{\circ}$ C with 100 μ L of the primary antibody (Alexa Fluor-coupled ZO-1)

195 in PBS containing 0.5% goat serum and 0.05% Triton X-100. The antibody was used in 1:100
196 dilution. The next day, cells were washed thrice with 300 μ L of 0.1% Triton X-100 in PBS for
197 5 min each and then incubated for 5 min with 300 μ L of 10.9 μ M DAPI in PBS. After three
198 final washing steps with PBS for 5 min each, the membranes containing the stained cells were
199 cut out of the supports, mounted on microscope slides using the ProLong® Gold antifade
200 reagent (Life Technologies, Carlsbad, CA, United States) and immediately investigated on a
201 Leica SP5 Laser Scanning Confocal Microscope (Leica, Heerbrugg, Switzerland).

202

203 Uptake for PS-NPs was investigated using the following protocol: After incubation with PS-
204 NPs, cells were washed thrice with 300 μ L L-15/ex and then incubated for 1 h with 300 μ L of
205 10.9 μ M DAPI in L-15/ex in the dark. Cells were washed again with 300 μ L L-15/ex and then
206 incubated for 8 min with 300 μ L of 7.5 μ g/mL CellMask® in L-15/ex in the dark. After two
207 additional washing steps with 300 μ L L-15/ex, cells were mounted on microscope slides and
208 investigated immediately by confocal microscopy as described above.

209

210 *Statistical evaluation*

211 If not stated otherwise, data in figures or tables represent mean value \pm standard deviation of
212 three individual experiments, performed with different passages of RTgutGC cells. Pictures of
213 stained cells show representative images of an experiment that was reproduced at least two
214 times with different passages of RTgutGC cells. Statistical analysis of two sets of data was
215 performed using unpaired *t*-test. Statistical analysis between groups of data was performed
216 using ANOVA with Bonferroni's *post hoc* test. $p > 0.05$ was considered as not significant.

217

218

219 **Results and Discussion**

220

221 **Nanoparticle characterization**

222 Fluorescent polystyrene nanoparticles (PS-NPs) were used as a model to study the uptake and
223 translocation of nanoparticles in the fish intestinal barrier. These particles were used earlier on
224 Caco-2 cells¹⁶ and have the advantage that they are (i) easy to quantify, (ii) non-dissolving and
225 (iii) non-toxic to the cells. According to the supplier, the PS-NPs have a diameter of 50 nm and
226 a carboxylated (negatively charged) surface. The aqueous stock solution of 25 g/L PS-NPs
227 contained 3.64×10^{14} particles/mL. When diluted to 10 mg/L (1.456×10^{11} particles/mL) in
228 water, PS-NPs had an average hydrodynamic diameter of 73 ± 18 nm and a zeta-potential of
229 -51 ± 1 mV (Table 1). Both values did not significantly change during at least 24 h of
230 incubation, demonstrating the stability of diluted, negatively charged PS-NPs in water. When
231 diluted in the different exposure media (see supporting information for media composition), PS-
232 NPs form slightly larger agglomerates with a maximum of 166 ± 23 nm determined after 24 h
233 (Table 1). However, PS-NPs still remained in the nanometer range and no precipitation was
234 observed. The zeta-potential of PS-NPs diluted in exposure media remained negative, but with
235 lower absolute values than in water (Table 1). This observation is likely due to the formation of
236 counter ion shells and/or a protein corona around the nanoparticles surface, thereby shielding
237 some of the original negative charge of the PS-NPs^{22, 23}.

238

239 **Intestinal barrier model characterization**

240 The rainbow trout intestinal cell line, RTgutGC²¹, was used as a model system for fish intestinal
241 cells. For establishing an intestinal barrier, RTgutGC cells were seeded on permeable
242 membrane supports (transwell inserts) with pore sizes of 0.4, 1 or 3 μm and grown to

243 confluency, leading to a two-compartment model consisting of an apical (upper) and a
244 basolateral (lower) compartment and a cell monolayer comprising the biological barrier (Fig.
245 1A,B). The reason for choosing different pore sizes was to evaluate how cell growth is affected
246 by the pores and how the membrane alone (without cells) influences the translocation of PS-
247 NPs by simple diffusion.

248

249 Cells developed a transepithelial electrical resistance (TEER) of $33 \pm 3 \Omega \times \text{cm}^2$ (0.4 μm pore-
250 size), $30 \pm 2 \Omega \times \text{cm}^2$ (1 μm pore-size) or $35 \pm 3 \Omega \times \text{cm}^2$ (3 μm pore-size) after 5 weeks of
251 culture (Fig. 1C). These TEER-values are much lower than those obtained on the frequently
252 used Caco-2 cell line, which develops a TEER in the range of 500-1000 $\Omega \times \text{cm}^2$ when cultured
253 on permeable membrane supports²⁴. According to the classification by Claude and
254 Goodenough²⁵, the epithelium formed by RTgutGC cells has to be considered 'leaky'. Indeed,
255 the TEER of RTgutGC cells is comparable to the TEER values observed in freshly isolated
256 sections of the Atlantic salmon, *Salmo salar*²⁶. Cells grow comparatively well on all
257 membranes reaching slightly higher TEER values on membranes with 3 μm pore-size. A
258 possible explanation for this finding is the ability of the cells to migrate through the larger 3 μm
259 pores and thus grow on the other side of the membrane (see supporting information).

260

261 RTgutGC cells grow on all membranes as a monolayer and express the tight junction protein
262 ZO-1 as shown by confocal microscopy (Fig. 1D-F). Thus, all types of membranes investigated
263 were suitable to establish RTgutGC cell monolayers and thereby establish a two-compartment
264 intestinal barrier model. Three weeks were chosen as minimum culture time for RTgutGC cells
265 before using them for investigation of uptake and translocation of nanoparticles. This decision
266 was made based on the microscopy images and TEER-data (Fig. 1C-F) which both demonstrate
267 that the model-epithelium has functional properties reflecting the *in vivo* epithelium.

268

269 **RTgutGC cells take up PS-NPs but form a barrier for translocation**

270 In order to study the uptake of PS-NPs into RTgutGC cells and the translocation of PS-NPs
271 through the intestinal barrier, the cells were incubated with PS-NPs in exposure medium (L-
272 15/ex) on the apical side and complete medium (L-15/FBS) on the basolateral side. The
273 composition of L-15/ex is very similar to that proposed as fish gut lumen surrogate²⁷, while the
274 serum containing complete medium (L-15/FBS), which was provided in the bottom
275 compartment, mimics the interior facing side of the epithelium. After incubation of RTgutGC
276 cells with 10 mg/L PS-NPs (4.368×10^{10} particles) for 24 h, more than 80% of the applied
277 particles remain in the apical compartment (Fig. 2A). However, RTgutGC cells accumulate
278 between 3.9 and 7.2×10^9 particles in the cellular compartment, which accounts for around 9-
279 16% of the total applied PS-NPs (Fig. 2B). Hardly any PS-NPs were detected in the basolateral
280 compartment, indicating that translocation of PS-NPs through the epithelium was very low (Fig.
281 2C). In order to prove that this is an effect of the cells forming an effective barrier, cell-free
282 membranes were treated identically and PS-NP contents in the different compartments were
283 determined (white bars in Fig. 2). Here, translocation of PS-NPs to the basolateral compartment
284 was detectable for the membranes with 1 and 3 μm pore-sizes. For membranes with 3 μm pore-
285 size, $8 \pm 5 \times 10^9$ particles translocated to the basolateral compartment which accounts for 18%
286 of the total applied particles. This clearly demonstrates that particle translocation through the
287 membranes is possible and that RTgutGC cells form a barrier, strongly reducing this
288 translocation. It further demonstrates the importance of choosing membranes with appropriate
289 pore-sizes that allow the diffusion of nanoparticles to the basolateral compartment.

290

291 The findings presented here support the results obtained earlier on iron oxide nanoparticles and
292 Caco-2 cells¹⁹. However, the results contrast the findings by Koeneman and colleagues who

293 showed that TiO₂ nanoparticles were able to penetrate through a Caco-2 intestinal barrier
294 model¹⁴. This is an interesting result especially considering the fact that Caco-2 cells are known
295 to develop a much tighter epithelium indicated by higher TEER values ($>250 \Omega \times \text{cm}^2$)¹⁴.
296 However, it has to be noted here that a direct comparison between PS-NPs and metal oxide NPs
297 can be hampered by the fact that ions, potentially released from the metal-based nanoparticles,
298 will be transported differently than the particles themselves. PS-NPs also have been shown to
299 be translocated across Caco-2 monolayers to a very low extent (less than 0.5%),¹⁵ and Caco-
300 2/HT29-MTX co-cultures to a larger extent¹⁶. However, it has to be noted that in the second
301 report, also M cells were present in the system which are known to be specialized for
302 transepithelial transport processes¹⁸.

303

304 To further confirm the accumulation of PS-NPs by our fish intestinal barrier model, fluorescent
305 microscopy images were taken after incubation of the cells for 24 h with 100 mg/L PS-NPs
306 (4.368×10^{11} particles). This higher concentration was chosen in order to achieve a better
307 visualization of PS-NPs in the images. Cell membranes were stained with CellMask® and
308 nuclei were counterstained with DAPI (Fig. 3). Green fluorescence indicated the presence of
309 PS-NPs, which were present as both, large and small agglomerates located either as precipitates
310 on the cell layer (white ellipses in Fig. 3A-E) or intracellular (white arrows in Fig. 3B-F) in the
311 perinuclear region. Thus, microscopy clearly supports our hypothesis that RTgutGC cells are
312 able to internalize PS-NPs, probably via endocytotic uptake mechanisms as shown earlier for
313 TiO₂ nanoparticles in perfused intestine of rainbow trout¹².

314

315 **Concentration-, temperature- and time-dependency of uptake and translocation of PS-**
316 **NPs**

317 The 3 μm pore-size membranes were chosen to explore the mechanisms of uptake and
318 translocation of PS-NPs in the rainbow trout intestinal barrier model in more detail. After 24 h
319 incubation of RTgutGC cells with different concentrations of PS-NPs at 19 $^{\circ}\text{C}$, a concentration-
320 dependent accumulation of particles was observed (Fig. 4C). The maximal amounts of
321 accumulated PS-NPs were $3.8 \pm 0.5 \times 10^{10}$ or $5.6 \pm 0.5 \times 10^{10}$ particles for extracellular
322 exposure concentrations of 30 or 100 mg/L, respectively. When the incubation was performed
323 at 4 $^{\circ}\text{C}$, the number of accumulated particles was significantly lower, reaching only $4.6 \pm 0.7 \times$
324 10^9 (30 mg/L) or $1.1 \pm 0.2 \times 10^{10}$ (100 mg/L) particles in the cellular compartment (Fig. 4C).
325 Together with the results from microscopy (Fig. 3), these data strongly corroborate our
326 hypothesis of energy-dependent uptake processes, more specifically endocytosis involved in
327 PS-NP accumulation by RTgutGC cells as shown earlier for different types of NPs on different
328 types of mammalian cells^{15, 28, 29}.

329

330 Besides particle accumulation, also the amount of translocated PS-NPs to the basolateral
331 compartment was strongly dependent on the concentration of applied PS-NPs and the
332 incubation temperature (Fig. 4E). After 24 h incubation, $1.3 \pm 0.2 \times 10^9$ or $3.8 \pm 0.7 \times 10^9$
333 particles were translocated through the epithelium for exposure concentrations of 30 or 100
334 mg/L PS-NPs at 19 $^{\circ}\text{C}$, respectively. However, these values account only for about 1% of the
335 applied PS-NPs. When the incubation temperature was lowered to 4 $^{\circ}\text{C}$, the amount of
336 translocated PS-NPs was detectable (detection limit around 1×10^8 particles/mL) only for the
337 highest applied concentration (100 mg/L) and accounted for $2.8 \pm 0.7 \times 10^8$ particles in the
338 basolateral compartment. In contrast, when empty membranes were incubated with PS-NPs, a
339 concentration-dependent but temperature-independent translocation of particles was measured
340 (Fig 4F). The TEER of RTgutGC cells did not change during the incubation with the different
341 PS-NP concentrations indicating that the integrity of the epithelium is not affected by the

342 incubation conditions (supplementary figure S3). Taken together, these results show that the
343 translocation of PS-NPs through the intact epithelial barrier is possible to a low extent when
344 PS-NPs are applied in high concentrations. The temperature dependency of this translocation
345 further supports the hypothesis that energy-dependent processes such as endocytotic uptake of
346 PS-NPs on the apical side and a subsequent release of PS-NPs on the basolateral side are
347 involved¹⁵.

348

349 The hypothesis of an active apical uptake and basolateral release of PS-NPs is also supported
350 by the results of the time-dependency of PS-NP translocation in RTgutGC cells (Fig. 5). After
351 incubation of RTgutGC cells with 10 mg/L PS-NPs, translocation of particles was hardly
352 detectable during the first 8 h of incubation, but then increased to $1.3 \pm 1.1 \times 10^9$, $2.0 \pm 0.7 \times$
353 10^9 and $4.9 \pm 3.5 \times 10^9$ particles for 24, 72 and 168 h, respectively (Fig 5E). In parallel, the
354 amount of accumulated PS-NPs in the cells increased strongly, leading to a maximum of $2.6 \pm$
355 2.9×10^{10} particles after 168 h incubation (Fig. 5C). This strong accumulation of PS-NPs by the
356 cells, accompanied by the delayed increase in basolateral particle contents, suggest a complex
357 transport-mechanism of PS-NPs involving apical uptake and basolateral release of particles.

358

359 When empty (cell-free) membranes were incubated with PS-NPs, no further translocation of
360 particles was detectable for incubation times longer than 24 h (Fig. 5F). A possible explanation
361 of this finding could be the formation of larger agglomerates of PS-NPs during the 7 day
362 incubation period. At this time point, particle agglomerates became visible by the eye, which
363 indicates that they are micrometer sized (and therefore out of range of proper investigation by
364 DLS measurements). Thus, due to the large size, agglomerates are likely no longer able to
365 penetrate the pores of the membrane. After all, this only occurred in the absence of cells which
366 further supports the hypothesis of an active transport of PS-NPs by the cells.

367

368 **Conclusions**

369 In conclusion, we present a novel two-compartment intestinal barrier model using the rainbow
370 trout intestinal cell-line, RTgutGC, and establish its potential for investigation of nanoparticle
371 translocation through the intestinal epithelium using fluorescent polystyrene nanoparticles (PS-
372 NPs) as a model nanoparticle. RTgutGC cells successfully grow on permeable membrane
373 supports with different pore-sizes and we show that the selection of membranes with
374 appropriate pore-sizes is a crucial step in developing a model for studying nanoparticle
375 transport. In addition, we demonstrate the barrier function of RTgutGC cells, with the barrier
376 strongly reducing the translocation of PS-NPs to the basolateral compartment. The here
377 presented model is the first *in vitro* model developed from fish cells for studying nanoparticle
378 transport across the intestinal barrier. Its great potential lies in the fact that it can be used for
379 rapid investigation of nanoparticle uptake and translocation in fish intestinal epithelial cells
380 under different experimental conditions. Thus the present model also has potential for high-
381 throughput screening in a tiered testing approach.

382 Future studies with the model could be designed in a way that further approaches the situation
383 *in vivo*. For example, nanoparticles could be pre-incubated in acidic environments which
384 resemble the situation in the stomach before adding them to the *in vitro* intestinal barrier
385 system. Another approach to advance the model is the use of additional cells like enterocytes in
386 the epithelial layer or fibroblasts seeded on the basolateral side, which will then directly
387 encounter nanoparticles that crossed the epithelium.

388

389 *Acknowledgements*

390 This research has been supported by EU FP7 grant NanoValid no 263147. The authors would
391 like to thank Carolin Drieschner and Nadine Bramaz for first establishing the ZO-1 staining and
392 Dr. Matteo Minghetti for his help with the confocal microscopy.

393 References

- 394 1. B. K. Gaiser, T. F. Fernandes, M. A. Jepson, J. R. Lead, C. R. Tyler, M. Baalousha, A.
395 Biswas, G. J. Britton, P. A. Cole, B. D. Johnston, Y. Ju-Nam, P. Rosenkranz, T. M.
396 Scown and V. Stone, *Environmental toxicology and chemistry / SETAC*, 2012, **31**, 144-
397 154.
- 398 2. F. Gottschalk, T. Sun and B. Nowack, *Environ Pollut*, 2013, **181**, 287-300.
- 399 3. K. Schirmer, in *Frontiers of Neuroscience*, eds. J. R. Lead and E. Valsami-Jones,
400 Elsevier, Amsterdam, Netherlands, 2014, vol. 7, pp. 195-221.
- 401 4. L. Sigg, in *Comprehensive Water Quality and Purification*, ed. S. Ahuja, Elsevier,
402 Amsterdam, Netherlands, 2014, vol. 4, pp. 315-328.
- 403 5. R. D. Handy, G. Al-Bairuty, A. Al-Jubory, C. S. Ramsden, D. Boyle, B. J. Shaw and T.
404 B. Henry, *Journal of fish biology*, 2011, **79**, 821-853.
- 405 6. M. Munari, J. Sturve, G. Frenzilli, M. B. Sanders, A. Brunelli, A. Marcomini, M. Nigro
406 and B. P. Lyons, *Mutation research. Genetic toxicology and environmental*
407 *mutagenesis*, 2014, **775-776**, 89-93.
- 408 7. N. T. K. Vo, M. R. Bufalino, K. D. Hartlen, V. Kitaev and L. E. J. Lee, *In Vitro Cell Dev-*
409 *An*, 2014, **50**, 427-438.
- 410 8. Y. Yue, R. Behra, L. Sigg, P. Fernandez Freire, S. Pillai and K. Schirmer,
411 *Nanotoxicology*, 2014, DOI: 10.3109/17435390.2014.889236.
- 412 9. M. Grosell, A. P. Farrell and C. J. Brauner, *The multifunctional gut of fish*, Elsevier,
413 Amsterdam, Netherlands, 2011.
- 414 10. R. D. Handy, M. M. Musonda, C. Phillips and S. J. Falla, *The Journal of experimental*
415 *biology*, 2000, **203**, 2365-2377.
- 416 11. I. Hoyle and R. D. Handy, *Aquat Toxicol*, 2005, **72**, 147-159.

- 417 12. A. R. Al-Jubory and R. D. Handy, *Nanotoxicology*, 2013, **7**, 1282-1301.
- 418 13. I. J. Hidalgo, T. J. Raub and R. T. Borchardt, *Gastroenterology*, 1989, **96**, 736-749.
- 419 14. B. A. Koeneman, Y. Zhang, P. Westerhoff, Y. Chen, J. C. Crittenden and D. G. Capco,
420 *Cell Biol Toxicol*, 2010, **26**, 225-238.
- 421 15. B. He, P. Lin, Z. Jia, W. Du, W. Qu, L. Yuan, W. Dai, H. Zhang, X. Wang, J. Wang, X.
422 Zhang and Q. Zhang, *Biomaterials*, 2013, **34**, 6082-6098.
- 423 16. G. J. Mahler, M. B. Esch, E. Tako, T. L. Southard, S. D. Archer, R. P. Glahn and M. L.
424 Shuler, *Nat Nanotechnol*, 2012, **7**, 264-U1500.
- 425 17. A. des Rieux, V. Fievez, I. Theate, J. Mast, V. Preat and Y. J. Schneider, *European*
426 *journal of pharmaceutical sciences : official journal of the European Federation for*
427 *Pharmaceutical Sciences*, 2007, **30**, 380-391.
- 428 18. J. P. Kraehenbuhl and M. R. Neutra, *Annual review of cell and developmental biology*,
429 2000, **16**, 301-332.
- 430 19. B. H. Kenzaoui, M. R. Vila, J. M. Miquel, F. Cengelli and L. Juillerat-Jeanneret,
431 *International journal of nanomedicine*, 2012, **7**, 1275-1286.
- 432 20. W. Zhang, M. Kalive, D. G. Capco and Y. Chen, *Nanotechnology*, 2010, **21**, 355103.
- 433 21. A. Kawano, C. Haiduk, K. Schirmer, R. Hanner, L. E. J. Lee, B. Dixon and N. C. Bols,
434 *Aquacult Nutr*, 2011, **17**, E241-E252.
- 435 22. I. Lynch, A. Salvati and K. A. Dawson, *Nat Nanotechnol*, 2009, **4**, 546-547.
- 436 23. A. E. Nel, L. Madler, D. Velegol, T. Xia, E. M. Hoek, P. Somasundaran, F. Klaessig, V.
437 Castranova and M. Thompson, *Nature materials*, 2009, **8**, 543-557.
- 438 24. E. Liang, K. Chessic and M. Yazdanian, *Journal of pharmaceutical sciences*, 2000, **89**,
439 336-345.
- 440 25. P. Claude and D. A. Goodenough, *The Journal of cell biology*, 1973, **58**, 390-400.
- 441 26. K. Sundell, F. Jutfelt, T. Agustsson, R. E. Olsen, E. Sandblom, T. Hansen and B. T.
442 Bjornsson, *Aquaculture*, 2003, **222**, 265-285.
- 443 27. J. Genz, A. J. Esbaugh and M. Grosell, *Comparative Biochemistry and Physiology, Part*
444 *A*, 2011, **159**, 150-158.

- 445 28. M. Geppert, M. C. Hohnholt, K. Thiel, S. Nurnberger, I. Grunwald, K. Rezwani and R.
446 Dringen, *Nanotechnology*, 2011, **22**, 145101.
- 447 29. C. Petters, F. Bulcke, K. Thiel, U. Bickmeyer and R. Dringen, *Neurochemical research*,
448 2014, **39**, 372-383.

449

450 **Figure Legends:**

451 **Figure 1: Characterization of the two-compartment intestinal barrier model.** A: Scheme of
452 the two-compartment intestinal barrier model involving rainbow trout intestinal cells
453 (RTgutGC) seeded on permeable membrane supports with different pore-sizes (0.4, 1 or 3 μm).
454 B: Empty insert used as cell-free control throughout the experiments. C: Transepithelial
455 electrical resistance (TEER) of the cell epithelium during growth for up to 35 days on
456 membranes with the indicated pore-sizes. D-F: Confocal fluorescence microscopy images of
457 RTgutGC cells grown in permeable membrane supports with 0.4 μm (D), 1 μm (E) or 3 μm (F)
458 pore-size. The tight junction protein ZO-1 (green) and the nuclei (blue) were stained. The size-
459 bar in F applies to all images. The data in panel C represent mean values \pm SD of five to six
460 individual experiments performed on different passages of RTgutGC cells. Asterisks indicate
461 significant differences which were observed between 1 μm and 3 μm pore-size membranes.
462 $*p<0.05$; $**p<0.01$.}

463

464 **Figure 2: Uptake and translocation of PS-NPs in intestinal barrier model.** RTgutGC cells
465 were seeded on permeable membrane supports with the indicated pore-sizes, grown for three
466 weeks and then incubated with 10 mg/L PS-NPs for 24 h. After incubation, the apical (A),
467 cellular (B) and basolateral (C) PS-NPs contents were determined by fluorescence measurement
468 of the respective media or cell lysates (black bars). As a control, cell-free membranes were
469 treated and analyzed identically (white bars). The data represent mean values \pm SD of five

470 experiments performed individually on different passages of RTgutGC cells. Asterisks indicate
471 significant differences which were observed between RTgutGC cells and cell-free conditions.
472 * $p < 0.05$.

473

474 **Figure 3: Internalization of PS-NPs into RTgutGC cells.** The cells were seeded on
475 permeable membrane supports (3 μm pore-size), grown for three weeks and then incubated
476 with 100 mg/L PS-NPs for 24 h. After incubation, cell membranes were stained with
477 CellMask® (purple) and nuclei were stained with DAPI (blue). PS-NPs are shown in green and
478 are present as extracellular large agglomerates (white ellipses) or as smaller agglomerates
479 located in the cells (white arrows). The images A-H show a z -stack through a representative
480 section of cells with a z -distance of 1 μm between the individual images. The size bar in H
481 applies to all panels.

482

483 **Figure 4: Temperature and concentration dependency of the uptake and translocation of**
484 **PS-NPs in intestinal barrier model.** RTgutGC cells were seeded on permeable membrane
485 supports (3 μm pore-size), grown for three weeks and then incubated with 1-100 mg/L PS-NPs
486 for 24 h at 19 °C and 4 °C. After incubation, the apical, cellular and basolateral PS-NP content
487 was determined by fluorescence measurement of the respective media or cell lysates (A,C,E).
488 As a control, cell-free membranes were treated and analyzed identically (B,D,F). The data
489 represent mean values \pm SD of three experiments performed individually on different passages
490 of RTgutGC cells. Asterisks indicate significances of differences between incubation at 19 °C
491 and at 4 °C (* $p < 0.05$; ** $p < 0.01$; *** $p < 0.001$).

492

493 **Figure 5: Time dependency of the uptake and translocation of PS-NPs in intestinal barrier**
 494 **model.** RTgutGC cells were seeded on permeable membrane supports (3 μm pore-size), grown
 495 for three weeks and then incubated with 10 mg/L PS-NPs for up to 168 h. After incubation, the
 496 apical, cellular and basolateral PS-NP content was determined by fluorescence measurement of
 497 the respective media or cell lysates (A,C,E). As a control, cell-free membranes were treated and
 498 analyzed identically (B,D,F). The data represent mean values \pm SD of three experiments
 499 performed individually on different passages of RTgutGC cells.

500

501

502 **Table 1: Characterization of fluorescent polystyrene nanoparticles (PS-NPs).**

503

504 Medium	505 particle diameter (nm)		505 zeta potential (mV)	
	1 h	24 h	1 h	24 h
506 Water	73 \pm 18	78 \pm 13	-51 \pm 1	-54 \pm 7
507 L-15/ex	67 \pm 11	120 \pm 12	-24 \pm 1***	-26 \pm 1***
508 L-15/FBS	72 \pm 3	166 \pm 23**	-9 \pm 1***	-11 \pm 1***

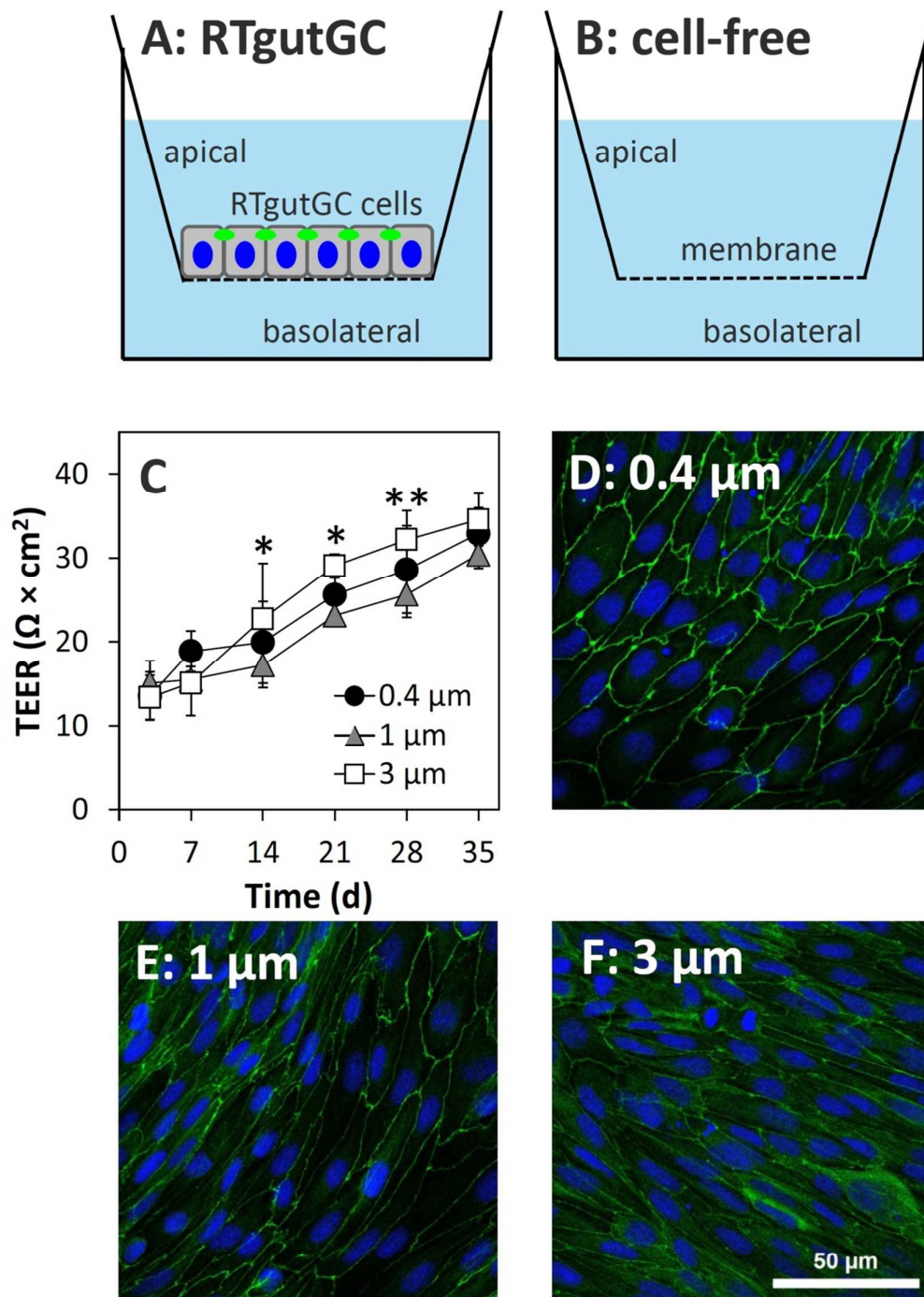
509

510 PS-NPs were diluted in water, L-15/ex, or L-15/FBS to a concentration of 10 mg/L and the
 511 hydrodynamic diameter and zeta-potential were determined 1 and 24 h after dilution. The data
 512 represent mean values \pm SD of three independent experiments. Asterisks indicate significant
 513 differences of values obtained in media samples compared to water. ** p <0.01; *** p <0.001.

514

515

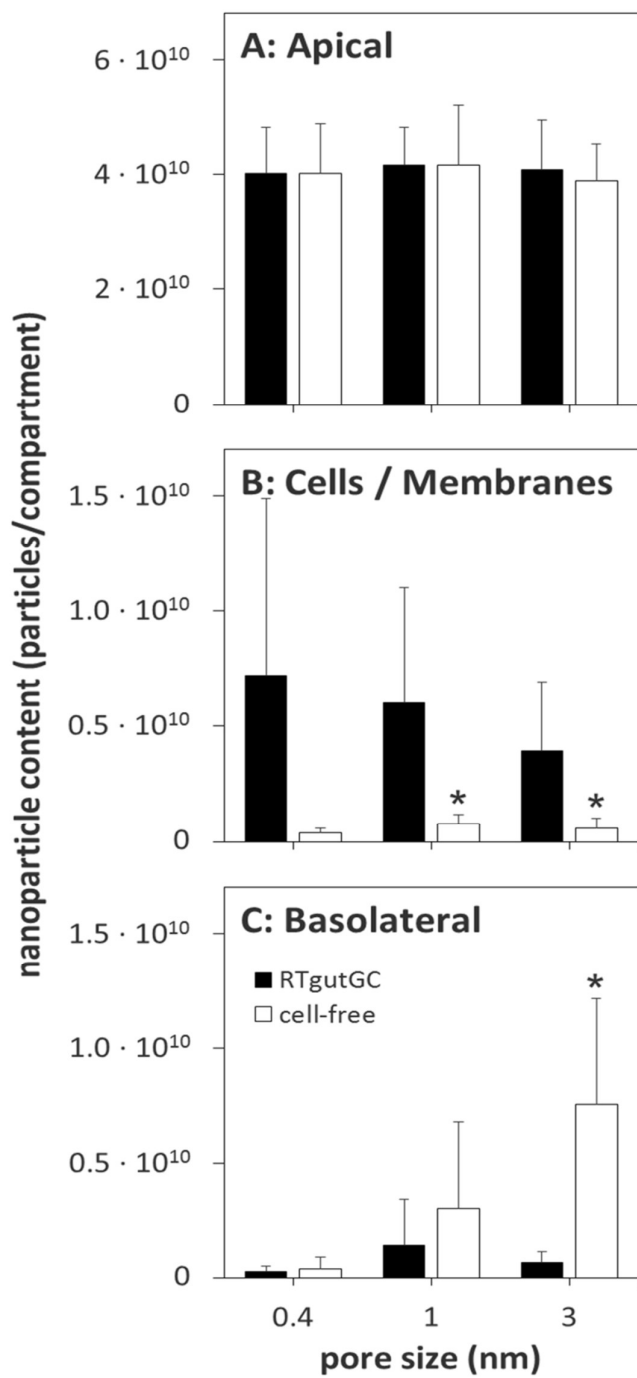
516 **Figure 1:**



517

518

519

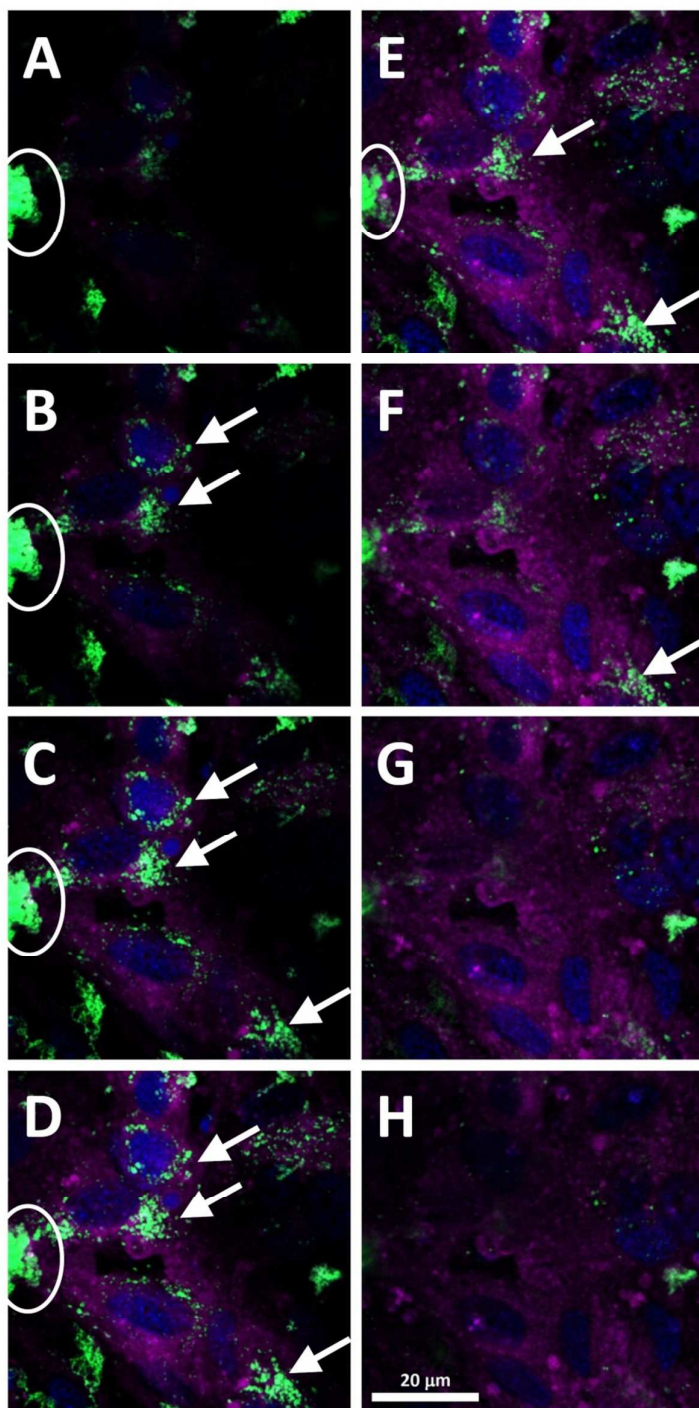
520 **Figure 2:**

521

522

523

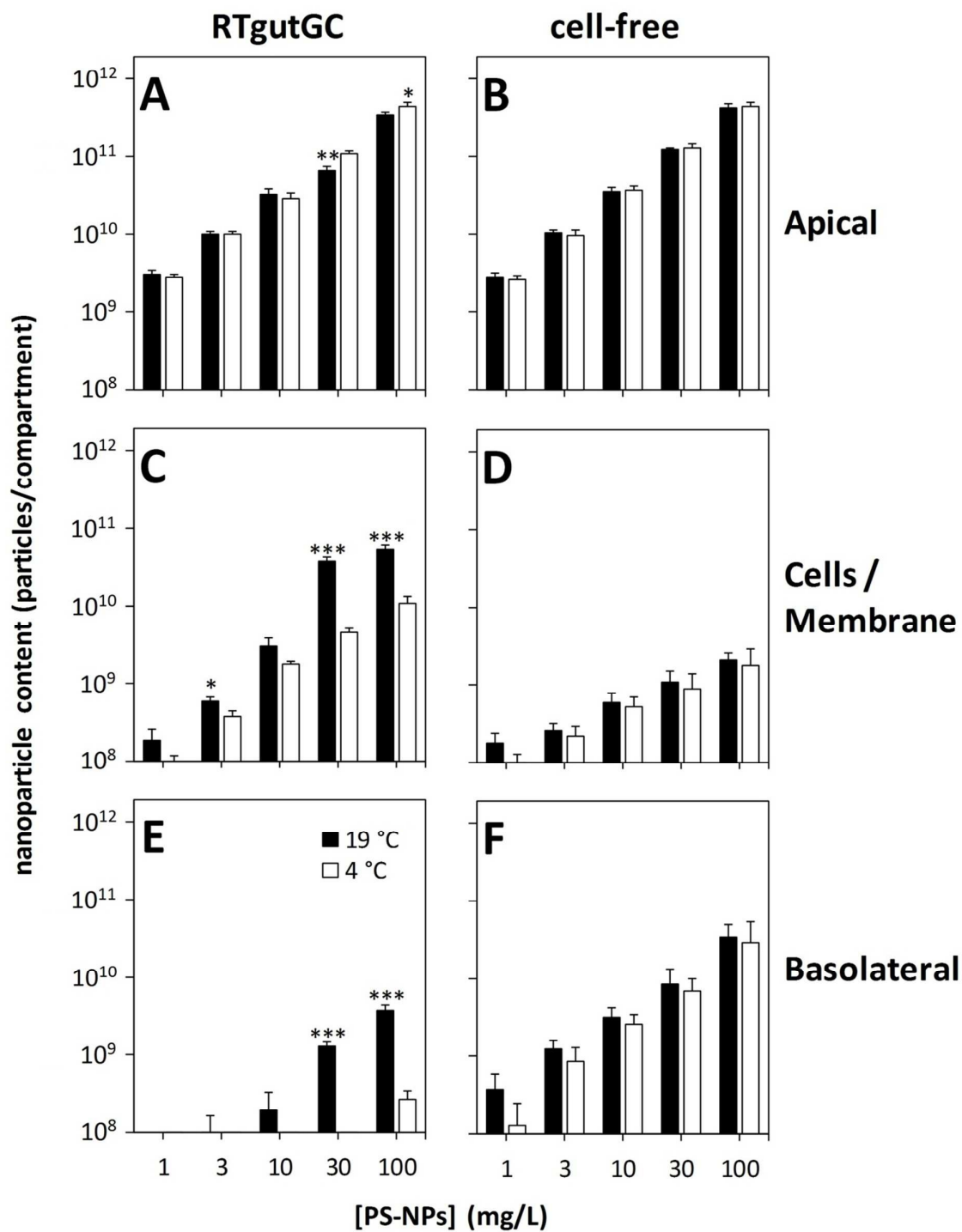
524

525 **Figure 3:**

526

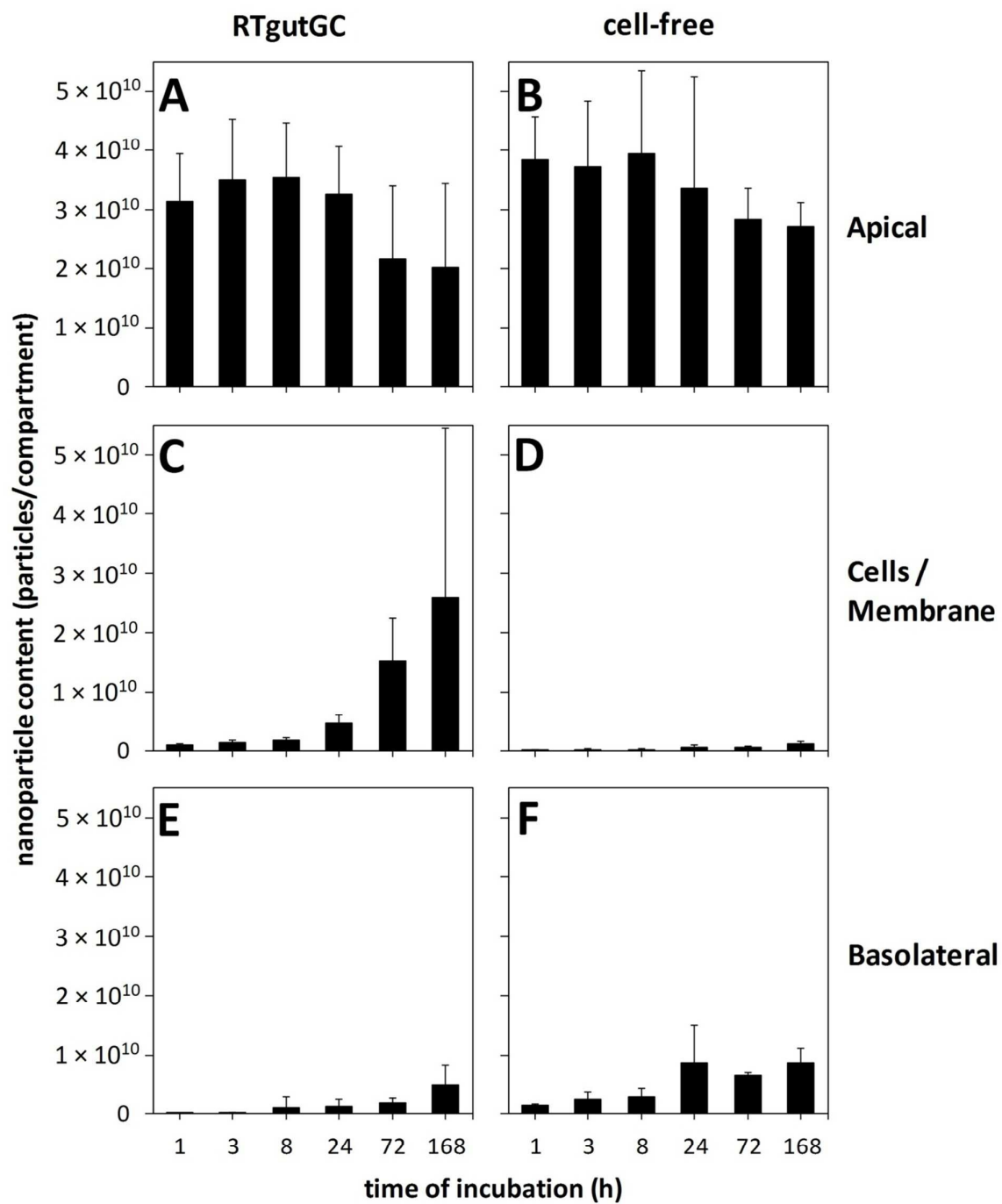
527

528

529 **Figure 4:**

530

531

532 **Figure 5:**

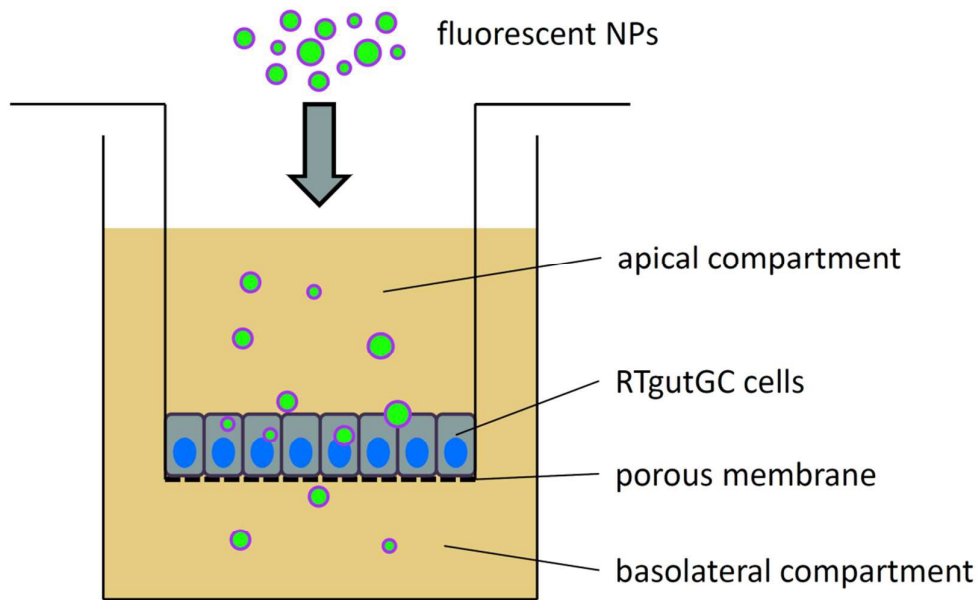
533

534

535

536

537 **Graphical abstract:**



538

539

540

541